NANO LETTERS
Letter
Cite This: Nano Lett. 2018, 18, 1972−1977
pubs.acs.org/NanoLett

Topological Electride Y_2C

Huaqing Huang,[†] Kyung-Hwan Jin,[†] Shunhong Zhang,[‡] and Feng Liu*[,†,§]

[†]Department of Materials Science and Engineering, University of Utah, Salt Lake City, Utah 84112, United States
[‡]Institute for Advanced Study, Tsinghua University, Beijing 100084, China
[§]Collaborative Innovation Center of Quantum Matter, Beijing 100084, China

Supporting Information

ABSTRACT: Two-dimensional (2D) electrides are layered ionic crystals in which anionic electrons are confined in the interlayer space. Here, we report a discovery of nontrivial $\mathbb{Z}_2$ topology in the electronic structures of 2D electride Y_2C. Based on first-principles calculations, we found a topological $\mathbb{Z}_2$ invariant of (1; 111) for the bulk band and topologically protected surface states in the surfaces of Y_2C, signifying its nontrivial electronic topology. We suggest a spin-resolved angle-resolved photoemission spectroscopy (ARPES) measurement to detect the unique helical spin texture of the spin-polarized topological surface state, which will provide characteristic evidence for the nontrivial electronic topology of Y_2C. Furthermore, the coexistence of 2D surface electride states and topological surface state enables us to explain the outstanding discrepancy between the recent ARPES experiments and theoretical calculations. Our findings establish a preliminary link between the electride in chemistry and the band topology in condensed-matter physics, which are expected to inspire further interdisciplinary research between these fields.

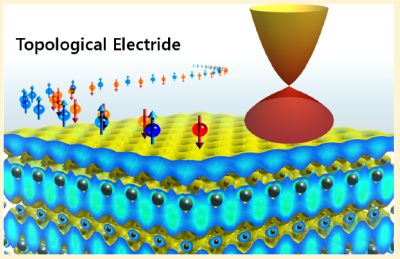

KEYWORDS: *Electronic topology, electride, yittrium hypocarbide, first-principles calculations, topological surface state*

Electrides are peculiar ionic solids in which electrons serve as anions.[1−4] Particularly the anionic electrons occupy void spaces instead of being specifically "assigned" to atoms or chemical bonds, leading to the notion of void quasiatoms (VQAs).[5−15] Electrides can be conveniently classified by the dimensionality of the void space confining the anionic electrons. For decades, all the discovered electrides were either 0D or 1D.[16−19] Very recently, Lee et al.[20] discovered the layered dicalcium nitride Ca_2N to be the first 2D electride with anionic electrons confined to the interlayer space between positively charged cations, which can move freely between the cation layers.[21−24] A recent angle-resolved photoemission spectroscopy (ARPES) experiment provides some evidence of the electride state in Y_2C.[25] It is also noted that there is a quantitative discrepancy between the theoretical calculation and experimental measurement of the electride bands, which remains an outstanding puzzle to be solved.

Additionally, the topological aspects of band structure have attracted considerable research interest in recent years.[26−33] Materials with nontrivial band topology exhibit unique properties such as robust metallic surface states of topological insulators due to the bulk-boundary correspondence.[34,35] Given the fact that anionic electrons form robust 2D electron gas in the surface of 2D electrides,[36] the following questions naturally arise: is there any nontrivial band topology in 2D electrides? If so, what is the interplay between the surface anionic electron and the topological surface state?

In this work, we demonstrate the existence of topological electride. We discover that the 2D electride Y_2C has a topologically nontrivial band structure based on first-principles calculations. The nontrivial band topology is identified by directly calculating the topological $\mathbb{Z}_2$ invariant and topological protected surface states. We further propose a spin-resolved ARPES experiment to measure the unique spin texture of topological surface state of Y_2C, which can provide a rather confirmative evidence for the nontrivial electronic topology of Y_2C. In addition, our discovery enabled us to resolve an outstanding discrepancy between the recent ARPES measurement and first-principles calculation, which can be attributed to the existence of topological surface state that was unknown before.

Yttrium hypocarbide (Y_2C) belongs to a family of rare-earth carbide with the anti-$CdCl_2$ type structure, similar to the structure of other electrides such as Ca_2N and Sr_2N.[37] As shown in Figure 1, Y_2C crystallizes in a trigonal $R\bar{3}m$ structure (D^5_{3d}, no. 166). The basic building block of Y_2C consists of a triple layer where C atoms are sandwiched by top and bottom Y layers. Each C atom occupies the center of an octahedron of Y atoms. The Y_2C crystal structure is formed by stacking these building blocks in an *ABC* sequence.

Our first-principles calculations are performed within the framework of density-functional theory as implemented in the Vienna ab initio simulation package[38] using the projector-augmented-wave method.[39] The exchange-correlation functional is treated using the Perdew−Burke−Ernzerhof-type[40] generalized gradient approximation. The cutoff energy for the

Received: December 22, 2017
Revised: February 19, 2018
Published: February 20, 2018

ACS Publications © 2018 American Chemical Society

DOI: 10.1021/acs.nanolett.7b05386
Nano Lett. 2018, 18, 1972−1977

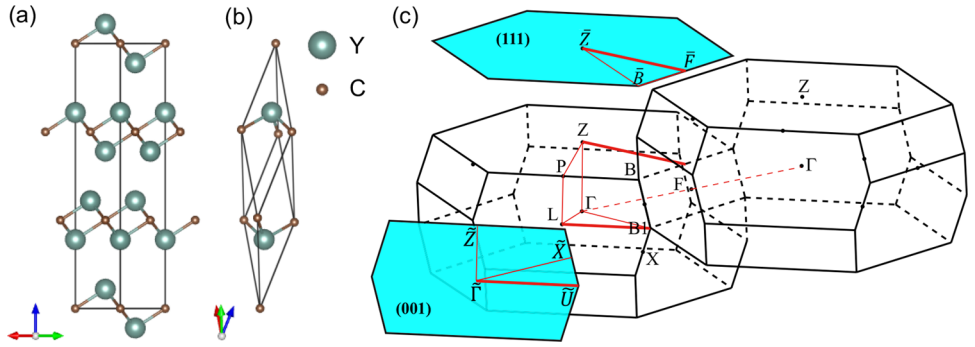

Figure 1. (a) Atomic structure of Y_2C with $R\bar{3}m$ (no. 166) symmetry in a trigonal conventional cell. (b) The rhombohedral primitive cell of Y_2C. (c) The Brillouin zone (BZ) of Y_2C and the projected surface BZs of the (111) and (100) surfaces.

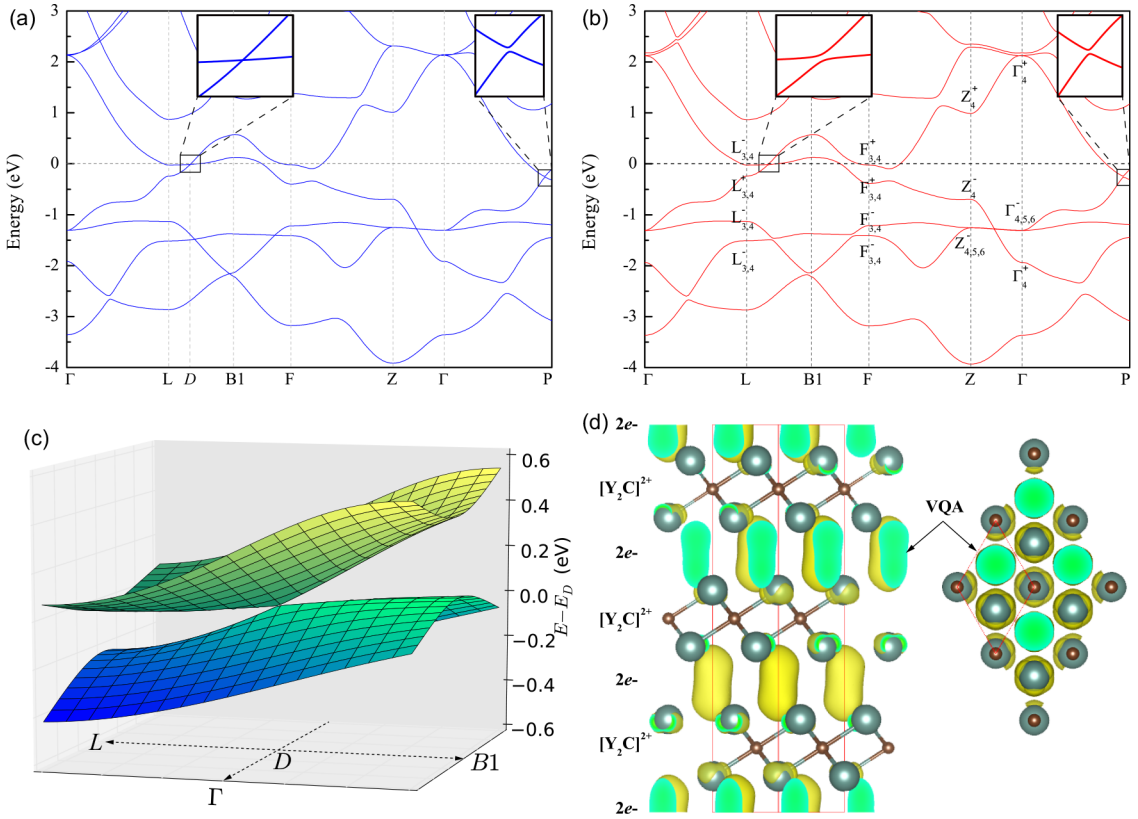

Figure 2. Band structure of Y_2C along the high-symmetry lines of the BZ (a) without and (b) with SOC. The insets show a zoomed-in view of the plot of the bands around the crossing or non-crossing points. (c) 3D band structures in the Γ-*L*-*B*1 plane around the nodal point *D* in the absence of SOC. (d) Side view and top view of the partial charge density for the states within 0.05 eV of the Fermi level. The VQAs are confined in the interlayer space and form a trigonal lattice.

plane-wave expansion is 400 eV, and a **k**-point mesh of 9 × 9 × 9 is used for Brillouin zone (BZ) integrations. The spin−orbit coupling (SOC) is included in the self-consistent calculations of electronic structures. We construct Wannier representations by projecting the Bloch states from the first-principles calculations of bulk materials onto Y *s* and *d* and C *p* atomic trial orbitals without an iterative maximal-localization procedure.[41−43] Based on Wannier representations, we further calculate the surface spectral function and Fermi surface using the surface Green's function method of semi-infinite systems.[44−46]

Figure 2a shows the calculated band structure of Y_2C in the absence of SOC. Both electron and hole pockets exist around the Fermi level, indicating that Y_2C is a metal. The conduction and valence bands are close to each other along some high-symmetry lines, such as the *L*-*B*1 and Γ-*P* lines. By carefully checking these bands, we found that the conduction and valence bands cross each other linearly in between *L* and *B*1 on the surface of the first BZ, leading to the formation of a band touching point (i.e., a node). Although the linear dispersion around the node resembles the character of a Dirac semimetal, the system is actually a nodal-line semimetal in the absence of SOC.[47,48] Namely, the band touching persists along a line in the 3D BZ forming closed nodal loops around the *L* points (see Figure S1). More importantly, the band dispersion around a node in the loops is over-tilted along one direction but untilted along others, which is the characteristic feature of the type-II nodal-line semimetals (see Figure 2c).[49−52] The calculated Fermi surface indicates that the nodes actually appear at the

DOI: 10.1021/acs.nanolett.7b05386
Nano Lett. 2018, 18, 1972−1977

contacts between electron and hole pockets and the Berry curvature distribution shows large values around these band touching points, implying that they are indeed the type-II nodal lines in the absence of SOC (see the Supporting Information for more details). According to our calculations, there are in total three type-II nodal lines in the BZ, which are related by the C_3 symmetry. Energetically, these type-II nodal lines are located very close to the Fermi energy E_F; for example, the energy of the nodal point D (E_D) is about −13 meV below E_F.

We next calculated the band structure of Y_2C in the presence of SOC as shown in Figure 2b. The conduction and valence bands avoid crossing due to the SOC effect, and the type-II nodal lines are gapped (see the insets of Figure 2b). Because of the coexistence of time reversal and inversion symmetries, every band is spin doubly degenerate. Hence, any band crossing in the electronic structure of Y_2C, if existed, would be 4-fold degenerate. Such high degeneracies are usually protected by extra crystalline symmetries, which only appear at high-symmetry points or lines such as the k_z axis with C_{3v} symmetry.[53] We checked the band structure along other high-symmetry lines and found the conduction and valence bands avoid crossing in all these lines. Hence, there is always a local gap between the conduction and valence bands at any arbitrary **k** point, although there is not a global gap in the entire BZ. This provides a possibility to define the topological $\mathbb{Z}_2$ invariant for the bands below the local gap, as discussed later.

We further calculated the partial charge density for states near the Fermi level, as shown in Figure 2d. It is clear that the VQAs composed of anionic electrons are confined inside the void space in between the cation layers. More interestingly, these VQAs form a trigonal lattice in the interlayer void space. Therefore, our results indicate that Y_2C is a 2D electride with semimetallic electride bands derived from anionic electrons confined in the interlayer space. This 2D electride character of Y_2C was also demonstrated by recent experiments.[11,25]

To identify the nontrivial electronic topology of Y_2C, we calculated the $\mathbb{Z}_2$ invariant. Because there is no global gap throughout the whole BZ, we consider the subspace spanned by the lowest N band, where N is the number of electrons per unit cell. These N bands are gapped from the higher bands everywhere in the entire BZ; hence, the topological $\mathbb{Z}_2$ invariant is well-defined in this subspace. Because the system has inversion symmetry, the $\mathbb{Z}_2$ indices can be determined from the parities of these N bands at time-reversal invariant momentum (TRIM) **k** points (see Table 1).[54,55] The parity product of bands below the gap is +1 at Z and −1 at other TRIMs; hence, the $k_{x,y,z} = \pi$ planes are topologically nontrivial with $\mathbb{Z}_2 = 1$, whereas the $k_{x,y,z} = 0$ planes are topologically trivial with $\mathbb{Z}_2 = 0$. We also checked the $\mathbb{Z}_2$ invariant using the hybrid Wannier charge-center approach,[56] which gives the same results. Therefore, the 2D electride Y_2C shares the same topological characters as strong topological insulators with the 3D $\mathbb{Z}_2$ invariant $(\nu_0; \nu_1\nu_2\nu_3) = (1; 111)$. Then, topological surface states are expected to appear on surfaces of Y_2C according to the bulk-boundary correspondence, as shown below.[34]

Table 1. Parity Products at TRIMs and the $\mathbb{Z}_2$ Index of Y_2C[a]

TRIM	Γ	$L \times 3$	$F \times 3$	Z
parity	−	−	−	+
plane ($i = x,y,z$)	$k_i = 0$	$k_i = \pi$	$(\nu_0; \nu_1\nu_2\nu_3)$	
$\mathbb{Z}_2$	0	1	(1; 111)	

[a]TRIMs are defined as $K_{n_1,n_2,n_3} = \frac{1}{2}(n_1\mathbf{G}_1 + n_2\mathbf{G}_2 + n_3\mathbf{G}_3)$, where $n_{1,2,3} = 0$ or 1 and $\mathbf{G}_1$, $\mathbf{G}_2$, and $\mathbf{G}_3$ are the primitive reciprocal lattice vectors.

For simplicity, we calculated the surface spectrum for the (100) surface of Y_2C. Figure 3a shows that the nontrivial surface states start from the nearly contacted points between bulk conduction and valence bands and disperse upward, merging into bulk-state continuum. The projected Fermi surface makes it clear that the nontrivial surface states emanate from the almost touched points between two Fermi pockets, cross each other in the bulk gapped region, and connect to one pocket (Figure 3b). Due to the mirror symmetry of the (100) surface, there are two sets of such surface states that appear in two sides of the central $\bar{\Gamma}$ point. These topological surface states, which are well-separated from bulk states, should be experimentally detectable by modern ARPES technique. These surface-state results agree with the $\mathbb{Z}_2$ invariant calculations, confirming again the nontrivial topological nature of Y_2C.

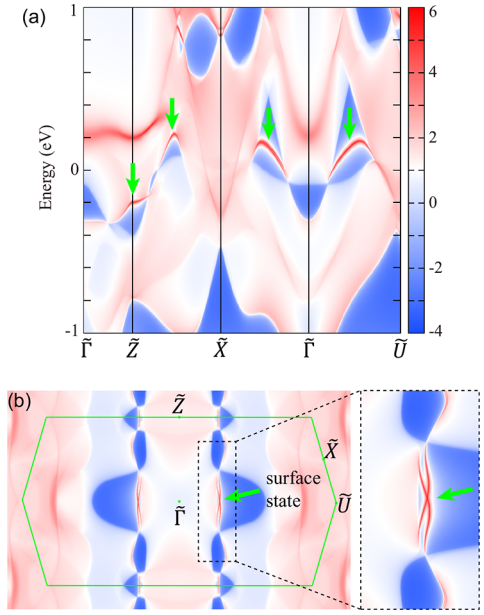

Figure 3. (a) Projected surface spectrum for the (100) surface of Y_2C, where topological surface states are around the Fermi level. (b) The projected Fermi surface of the (100) surface. The zoomed-in view of the plot shows the projected Fermi surface around the topological surface states, which are marked by green arrows.

Due to the layered structure of Y_2C, the Y terminated (111) surface is a natural cleaved facet of Y_2C, which is more easily accessible in experiments in comparison to the (100) surface. As a 2D electride, there should be 2D metallic electride states consisting of anionic electrons on the (111) surface of Y_2C.[36] However, the nontrivial bulk electronic topology guarantees the existence of topological surface states in this surface. The coexistence and interplay between the 2D surface electride states and topological surface states may give rise to rich physical properties and potential applications in topological electronics and electride-based devices.

We have calculated the surface electronic structure of the (111) surface of Y_2C as shown in Figures 4 and 5. The calculated surface spectrum agrees well with the recent ARPES measurements[25] in a large energy range (see Figure 5). Due to

DOI: 10.1021/acs.nanolett.7b05386
Nano Lett. 2018, 18, 1972−1977

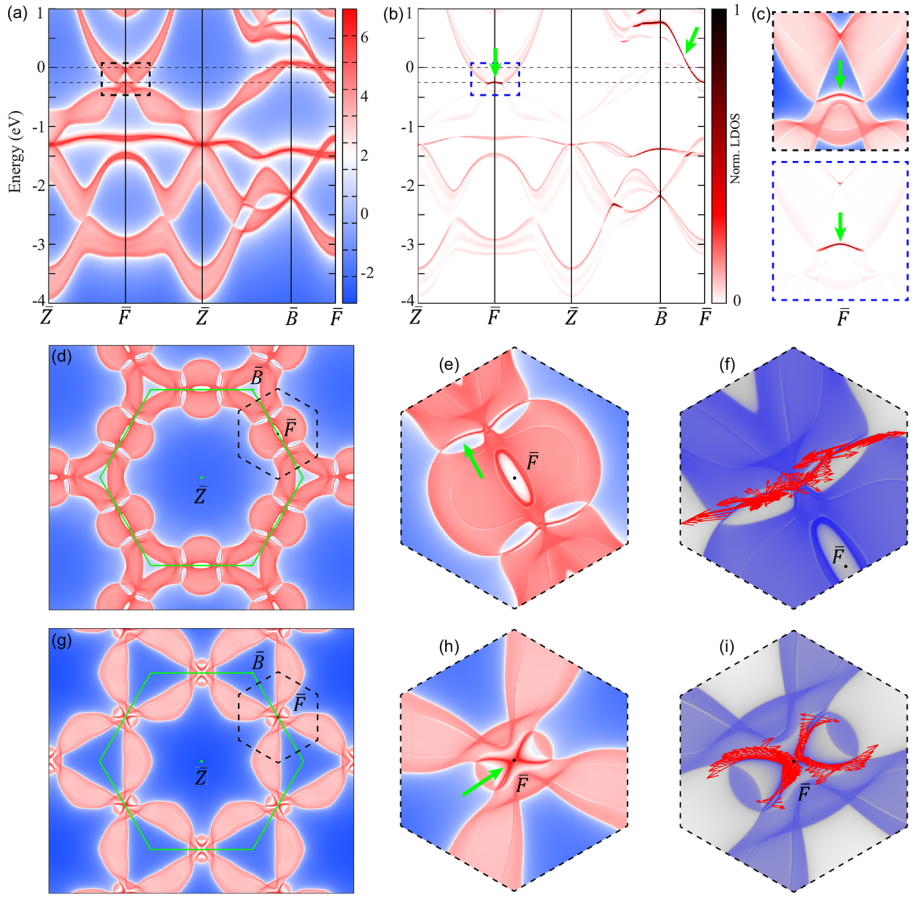

Figure 4. (a) Projected surface spectrum for the (111) surface of Y_2C. (b) The difference between surface and bulk spectrum for the (111) surface of Y_2C. (c) The zoomed-in image of the plot of the spectrum around the $\bar{F}$ point [the area marked by black and blue boxes in panels a and b, respectively. The green arrows mark topological surface states. (d) The isoenergy surface, (e) the zoomed-in image of the plot around $\bar{F}$, and (f) the in-plane spin texture of the surface state at E_F. (g) The isoenergy surface, (h) the zoomed-in image of the plot around $\bar{F}$, and (i) the in-plane spin texture of the surface state at $E_F - 0.25$ eV. The green hexagons in panels d and g represent the surface BZ.

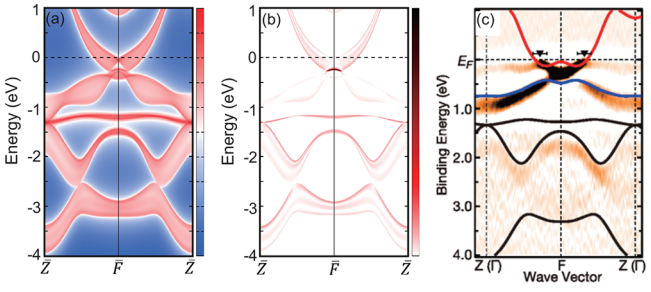

Figure 5. (a) Projected surface spectrum and (b) the difference between surface and bulk spectrum along the $\bar{Z}$-$\bar{F}$-$\bar{Z}$ path for the (111) surface of Y_2C. The surface state around $\bar{F}$ near the Fermi level is clearly visible. (c) Experimental band structure obtained by plotting the second derivative of the ARPES spectra acquired along the k path passing through the F point in the rhombohedral Brillouin zone for which ARPES measurements were carried out at $h\nu$ = 440 eV. The energy bands along the Z(Γ)-F-Z(Γ) direction calculated by the FLAPW method are superimposed by solid lines. Filled triangles indicate the Fermi momentum (k_F) determined by ARPES spectra. Panel c is reprinted in part with permission from ref 25. Copyright 2017 American Physical Society.

the nontrivial electronic topology of Y_2C, a topological surface state disperses downward from $\bar{B}$ to $\bar{F}$ crossing the Fermi level. There is also a piece of topological surface state connecting the electron and hole electride bands around the $\bar{F}$ point in the $\bar{Z}$-$\bar{F}$-$\bar{Z}$ path (see Figure 4a–c). Actually, this topological surface state already appears in previous ARPES results,[25] which causes a quantitative discrepancy between the experimental measurement and a simple bulk band calculation. We directly compared our results of surface state calculation with the ARPES spectrum.[25] As shown in Figure 5, the topological surface state around $\bar{F}$ near the Fermi level is clearly visible, which agrees well with the strong intensity of in-gap states in the ARPES measured band structure. The good agreement between the ARPES observations and our calculated topological surface states on the (111) surface resolve this outstanding discrepancy, which in turn provides additional evidence for the nontrivial electronic topology in the 2D electride Y_2C (see the Supporting Information for more details).

How to confirm that the experimentally observed states around the $\bar{F}$ point are caused by the nontrivial electronic topology of Y_2C instead of other possible reasons such as the correction from electron–electron interaction of Y 4*d* bands?[25] The answer is to use a spin-resolved ARPES technique, which enables the determination of the spin texture of the topological surface bands.[57−59] To illustrate this, we calculated the isoenergy contours of the projected surface spectrum at E_F and $E_F - 0.25$ eV, as shown in Figure 4d–i. By zooming in the states around $\bar{F}$, one can clearly see the topological surface states, although they only appear in the gapped regions of the bulk-state continuum. More interestingly, the topological

DOI: 10.1021/acs.nanolett.7b05386
Nano Lett. 2018, 18, 1972−1977

surface states are spin-polarized with helical spin textures due to the unique spin-momentum locking property in topological materials (see Figure 4f,i),[60−62] which is distinctively different from the spin-unpolarized electride bands[8,9] or the ferromagnetic instability.[63] The unique spin texture on the (111) surface of Y_2C is expected to be detected by spin-resolved AREPS measurement, which would provide the characteristic evidence for the nontrivial electronic topology in Y_2C.

The presence of topological surface states may give rise to anomalous magneto-transport properties. Also, due to the unique spin-momentum lacking properties, the topologically protected surface states are spin-polarized with helical spin textures, which are distinct from trivial surface state. These unique spin-polarized characteristics of topological surface states are expected to be observed by spin-resolved ARPES measurements and may have potential applications for devices employing spin-polarized transport[64,65] and spin Seeback effect.[66] Our findings may inspire further study of topological properties in other electrides. For example, we found that Sc_2C, Tb_2C, Dy_2C, and Ho_2C all have nontrivial band topology, which are in the Supporting Information. It is interesting to note that previously, topological states have been also predicted in Mxene[31] and transition metal intercalated graphene,[67] and in this sense, our current work enlarges the carbonated transition metal topological family.

In conclusion, we discover a topological 2D electride Y_2C by calculating the topological $\mathbb{Z}_2$ invariant and topological surface states based on first-principles calculations. Our finding, on the one hand, demonstrates new unknown electronic properties in electrides and, on the other hand, adds a unique class of members to the ever growing family of topological materials. It marries two research fields: the electride in chemistry and the band topology in condensed matter physics, which will stimulate highly interdisciplinary research in the future. For example, investigation of more electronic topology-related phenomena of electrides should be carried out, such as optical, transport and mangetoresponse behaviors. More candidate materials of topological electrides are expected to be found. The combination of nontrivial electronic topology and anionic electron states in electrides may also lead to potential applications in electride-based topological electronics and topological-related electride devices.

■ ASSOCIATED CONTENT

Supporting Information

The Supporting Information is available free of charge on the ACS Publications website at DOI: 10.1021/acs.nanolett.7b05386.

Additional details on computations; calculation of Berry curvature and $\mathbb{Z}_2$ invariants; structural information on Y_2C electride; nodal line distribution in the BZ; Fermi surface; Berry curvature distribution; Wannier interpolated band structure; evolution of Wannier charge centers; and other topological electrides including Sc_2C, Tb_2C, Dy_2C, and Ho_2C. (PDF)

■ AUTHOR INFORMATION

Corresponding Author

*E-mail: fliu@eng.utah.edu. Phone: 801-587-7719. Fax: 801-581-4816.

ORCID

Huaqing Huang: 0000-0002-0283-8603

Kyung-Hwan Jin: 0000-0002-5116-9987

Feng Liu: 0000-0002-3701-8058

Notes

The authors declare no competing financial interest.

■ ACKNOWLEDGMENTS

This work was support by U.S. DOE-BES (grant no. DE-FG02-04ER46148). The calculations were done on the CHPC at the University of Utah and DOE-NERSC.

■ REFERENCES

(1) Dye, J. L. *Science* **1990**, *247*, 663−668.
(2) Dye, J. L. *Science* **2003**, *301*, 607−608.
(3) Dye, J. L. *Acc. Chem. Res.* **2009**, *42*, 1564−1572.
(4) Ming, W.; Yoon, M.; Du, M.-H.; Lee, K.; Kim, S. W. *J. Am. Chem. Soc.* **2016**, *138*, 15336−15344.
(5) Redko, M. Y.; Jackson, J. E.; Huang, R. H.; Dye, J. L. *J. Am. Chem. Soc.* **2005**, *127*, 12416−12422.
(6) (a) Li, Z.; Yang, J.; Hou, J.; Zhu, Q. *J. Am. Chem. Soc.* **2003**, *125*, 6050−6051. (b) Li, Z.; Yang, J.; Hou, J.; Zhu, Q. *Chem. - Eur. J.* **2004**, *10*, 1592−1596.
(7) Zhao, S.; Kan, E.; Li, Z. *WIREs: Comput. Mol. Sci.* **2016**, *6*, 430−440.
(8) Inoshita, T.; Jeong, S.; Hamada, N.; Hosono, H. *Phys. Rev. X* **2014**, *4*, 031023.
(9) Tada, T.; Takemoto, S.; Matsuishi, S.; Hosono, H. *Inorg. Chem.* **2014**, *53*, 10347−10358.
(10) Druffel, D. L.; Kuntz, K. L.; Woomer, A. H.; Alcorn, F. M.; Hu, J.; Donley, C. L.; Warren, S. C. *J. Am. Chem. Soc.* **2016**, *138*, 16089−16094.
(11) Zhang, X.; Xiao, Z.; Lei, H.; Toda, Y.; Matsuishi, S.; Kamiya, T.; Ueda, S.; Hosono, H. *Chem. Mater.* **2014**, *26*, 6638−6643.
(12) Hou, J.; Tu, K.; Chen, Z. *J. Phys. Chem. C* **2016**, *120*, 18473−18478.
(13) Park, J.; Lee, K.; Lee, S. Y.; Nandadasa, C. N.; Kim, S.; Lee, K. H.; Lee, Y. H.; Hosono, H.; Kim, S.-G.; Kim, S. W. *J. Am. Chem. Soc.* **2017**, *139*, 615−618.
(14) Park, J.; Hwang, J.-Y.; Lee, K. H.; Kim, S.-G.; Lee, K.; Kim, S. W. *J. Am. Chem. Soc.* **2017***139*, 17277−17280.10.1021/jacs.7b10338
(15) Kim, S.; Song, S.; Park, J.; Yu, H. S.; Cho, S.; Kim, D.; Baik, J.; Choe, D.-H.; Chang, K. J.; Lee, Y. H.; Kim, S. W.; Yang, H. *Nano Lett.* **2017**, *17*, 3363.
(16) Ellaboudy, A.; Dye, J. L.; Smith, P. B. *J. Am. Chem. Soc.* **1983**, *105*, 6490−6491.
(17) Matsuishi, S.; Toda, Y.; Miyakawa, M.; Hayashi, K.; Kamiya, T.; Hirano, M.; Tanaka, I.; Hosono, H. *Science* **2003**, *301*, 626−629.
(18) Kim, S. W.; Shimoyama, T.; Hosono, H. *Science* **2011**, *333*, 71−74.
(19) Ichimura, A. S.; Dye, J. L.; Camblor, M. A.; Villaescusa, L. A. *J. Am. Chem. Soc.* **2002**, *124*, 1170−1171.
(20) Lee, K.; Kim, S. W.; Toda, Y.; Matsuishi, S.; Hosono, H. *Nature* **2013**, *494*, 336.
(21) Gregory, D. H.; Bowman, A.; Baker, C. F.; Weston, D. P. *J. Mater. Chem.* **2000**, *10*, 1635−1641.
(22) Fang, C.; de Wijs, G.; de Groot, R.; Hintzen, H.; de With, G. *Chem. Mater.* **2000**, *12*, 1847−1852.
(23) Walsh, A.; Scanlon, D. O. *J. Mater. Chem. C* **2013**, *1*, 3525−3528.
(24) Oh, J. S.; Kang, C.-J.; Kim, Y. J.; Sinn, S.; Han, M.; Chang, Y. J.; Park, B.-G.; Kim, S. W.; Min, B. I.; Kim, H.-D.; Noh, T. W. *J. Am. Chem. Soc.* **2016**, *138*, 2496−2499.
(25) Horiba, K.; Yukawa, R.; Mitsuhashi, T.; Kitamura, M.; Inoshita, T.; Hamada, N.; Otani, S.; Ohashi, N.; Maki, S.; Yamaura, J.-i.; Hosono, H.; Murakami, Y.; Kumigashira, H. *Phys. Rev. B: Condens. Matter Mater. Phys.* **2017**, *96*, 045101.
(26) Hasan, M. Z.; Kane, C. L. *Rev. Mod. Phys.* **2010**, *82*, 3045−3067.
(27) Qi, X.-L.; Zhang, S.-C. *Rev. Mod. Phys.* **2011**, *83*, 1057−1110.

DOI: 10.1021/acs.nanolett.7b05386
Nano Lett. 2018, 18, 1972−1977

(28) Kambe, T.; Sakamoto, R.; Kusamoto, T.; Pal, T.; Fukui, N.; Hoshiko, K.; Shimojima, T.; Wang, Z.; Hirahara, T.; Ishizaka, K.; Hasegawa, S.; Liu, F.; Nishihara, H. *J. Am. Chem. Soc.* **2014**, *136*, 14357−14360.
(29) Wang, Z.; Su, N.; Liu, F. *Nano Lett.* **2013**, *13*, 2842−2845.
(30) Zhang, L.; Wang, Z.; Huang, B.; Cui, B.; Wang, Z.; Du, S.; Gao, H.-J.; Liu, F. *Nano Lett.* **2016**, *16*, 2072−2075.
(31) Si, C.; Jin, K.-H.; Zhou, J.; Sun, Z.; Liu, F. *Nano Lett.* **2016**, *16*, 6584−6591.
(32) Huang, H.; Xu, Y.; Wang, J.; Duan, W. *WIREs: Comput. Mol. Sci.* **2017**, *7*, e1296.
(33) Wang, Z.; Jin, K.-H.; Liu, F. *WIREs: Comput. Mol. Sci.* **2017**, *7*, e1304.
(34) Halperin, B. I. *Phys. Rev. B: Condens. Matter Mater. Phys.* **1982**, *25*, 2185−2190.
(35) Huang, H.; Wang, Z.; Luo, N.; Liu, Z.; Lü, R.; Wu, J.; Duan, W. *Phys. Rev. B: Condens. Matter Mater. Phys.* **2015**, *92*, 075138.
(36) Zhao, S.; Li, Z.; Yang, J. *J. Am. Chem. Soc.* **2014**, *136*, 13313−13318.
(37) Atoji, M.; Kikuchi, M. *J. Chem. Phys.* **1969**, *51*, 3863−3872.
(38) Kresse, G.; Furthmüller, J. *Comput. Mater. Sci.* **1996**, *6*, 15.
(39) Blöchl, P. E. *Phys. Rev. B: Condens. Matter Mater. Phys.* **1994**, *50*, 17953−17979.
(40) Perdew, J. P.; Burke, K.; Ernzerhof, M. *Phys. Rev. Lett.* **1996**, *77*, 3865.
(41) (a) Marzari, N.; Vanderbilt, D. *Phys. Rev. B: Condens. Matter Mater. Phys.* **1997**, *56*, 12847−12865. (b) Souza, I.; Marzari, N.; Vanderbilt, D. *Phys. Rev. B: Condens. Matter Mater. Phys.* **2001**, *65*, 035109.
(42) Mostofi, A. A.; Yates, J. R.; Lee, Y.-S.; Souza, I.; Vanderbilt, D.; Marzari, N. *Comput. Phys. Commun.* **2008**, *178*, 685−699.
(43) Huang, H.; Liu, F. *Phys. Rev. B: Condens. Matter Mater. Phys.* **2017**, *95*, 201101.
(44) (a) López Sancho, M. P.; López Sancho, J. M.; Rubio, J. *J. Phys. F* **1984**, *14*, 1205. (b) López Sancho, M. P.; López Sancho, J. M.; Rubio, J. *J. Phys. F* **1985**, *15*, 851.
(45) Huang, H.; Jin, K.-H.; Liu, F. *Phys. Rev. B: Condens. Matter Mater. Phys.* **2017**, *96*, 115106.
(46) Wu, Q.; Zhang, S.; Song, H.-F.; Troyer, M.; Soluyanov, A. A. *Comput. Phys. Commun.* **2018**, *224*, 405−416.
(47) Park, C.; Kim, S. W.; Yoon, M. *Phys. Rev. Lett.* **2018**, *120*, 026401.
(48) Huang, H.; Liu, J.; Vanderbilt, D.; Duan, W. *Phys. Rev. B: Condens. Matter Mater. Phys.* **2016**, *93*, 201114.
(49) Li, S.; Yu, Z.-M.; Liu, Y.; Guan, S.; Wang, S.-S.; Zhang, X.; Yao, Y.; Yang, S. A. *Phys. Rev. B: Condens. Matter Mater. Phys.* **2017**, *96*, 081106.
(50) Zhang, X.; Jin, L.; Dai, X.; Liu, G. *J. Phys. Chem. Lett.* **2017**, *8*, 4814−4819.
(51) Chang, T.-R.; Pletikosic, I.; Kong, T.; Bian, G.; Huang, A.; Denlinger, J.; Kushwaha, S. K.; Sinkovic, B.; Jeng, H.-T.; Valla, T.; Xie, W.; Cava, R. J.2017, *ArXiv:1711.09167*. arXiv.org e-Print archive. https://export.arxiv.org/pdf/1711.09167 (accessed Nov 26, 2017).
(52) He, J.; Kong, X.; Wang, W.; Kou, S.-P.2017, *ArXiv:1709.08287*. arXiv.org e-Print archive. https://arxiv.org/abs/1709.08287 (accessed Sep 27, 2017).
(53) Huang, H.; Zhou, S.; Duan, W. *Phys. Rev. B: Condens. Matter Mater. Phys.* **2016**, *94*, 121117.
(54) Fu, L.; Kane, C. L. *Phys. Rev. B: Condens. Matter Mater. Phys.* **2007**, *76*, 045302.
(55) Fu, L.; Kane, C. L.; Mele, E. J. *Phys. Rev. Lett.* **2007**, *98*, 106803.
(56) Soluyanov, A. A.; Vanderbilt, D. *Phys. Rev. B: Condens. Matter Mater. Phys.* **2011**, *83*, 235401.
(57) Hsieh, D.; Xia, Y.; Wray, L.; Qian, D.; Pal, A.; Dil, J. H.; Osterwalder, J.; Meier, F.; Bihlmayer, G.; Kane, C. L.; Hor, Y. S.; Cava, R. J.; Hasan, M. Z. *Science* **2009**, *323*, 919−922.
(58) Pan, Z.-H.; Vescovo, E.; Fedorov, A. V.; Gardner, D.; Lee, Y. S.; Chu, S.; Gu, G. D.; Valla, T. *Phys. Rev. Lett.* **2011**, *106*, 257004.
(59) Souma, S.; Kosaka, K.; Sato, T.; Komatsu, M.; Takayama, A.; Takahashi, T.; Kriener, M.; Segawa, K.; Ando, Y. *Phys. Rev. Lett.* **2011**, *106*, 216803.
(60) Zhang, W.; Yu, R.; Zhang, H.-J.; Dai, X.; Fang, Z. *New J. Phys.* **2010**, *12*, 065013.
(61) Liu, C.-X.; Qi, X.-L.; Zhang, H.; Dai, X.; Fang, Z.; Zhang, S.-C. *Phys. Rev. B: Condens. Matter Mater. Phys.* **2010**, *82*, 045122.
(62) Yazyev, O. V.; Moore, J. E.; Louie, S. G. *Phys. Rev. Lett.* **2010**, *105*, 266806.
(63) Inoshita, T.; Hamada, N.; Hosono, H. *Phys. Rev. B: Condens. Matter Mater. Phys.* **2015**, *92*, 201109.
(64) Tian, J.; Childres, I.; Cao, H.; Shen, T.; Miotkowski, I.; Chen, Y. P. *Solid State Commun.* **2014**, *191*, 1−5.
(65) Tian, J.; Miotkowski, I.; Hong, S.; Chen, Y. P. *Sci. Rep.* **2015**, *5*, 14293.
(66) Jiang, Z.; Chang, C.-Z.; Masir, M. R.; Tang, C.; Xu, Y.; Moodera, J. S.; MacDonald, A. H.; Shi, J. *Nat. Commun.* **2016**, *7*, 11458.
(67) Zhou, J.; Jena, P. *Phys. Rev. B: Condens. Matter Mater. Phys.* **2017**, *95*, 081102.

DOI: 10.1021/acs.nanolett.7b05386
Nano Lett. 2018, 18, 1972−1977